Journal Pre-proofs

Combining triboelectric nanogenerator with piezoelectric effect for optimizing Schottky barrier height modulation

Luming Zhao, Hu Li, Jianping Meng, Yan Zhang, Hongqin Feng, Yuxiang Wu, Zhou Li

PII: S2095-9273(21)00230-9
DOI: https://doi.org/10.1016/j.scib.2021.03.013
Reference: SCIB 1410

To appear in: *Science Bulletin*

Received Date: 15 December 2020
Revised Date: 5 February 2021
Accepted Date: 1 March 2021

Please cite this article as: L. Zhao, H. Li, J. Meng, Y. Zhang, H. Feng, Y. Wu, Z. Li, Combining triboelectric nanogenerator with piezoelectric effect for optimizing Schottky barrier height modulation, *Science Bulletin* (2021), doi: https://doi.org/10.1016/j.scib.2021.03.013

Article

Received 15 December 2020

Received in revised form 5 February 2021

Accepted 1 March 2021

Combining triboelectric nanogenerator with piezoelectric effect for optimizing Schottky barrier height modulation

Luming Zhao [a,b,c], *Hu Li* [a], *Jianping Meng* [a,c], *Yan Zhang* [d, e], *Hongqin Feng* [a,c], *Yuxiang Wu* [f,*], *Zhou Li* [a,c,d,*]

[a] CAS Center for Excellence in Nanoscience, Beijing Key Laboratory of Micro-nano Energy and Sensor, Beijing Institute of Nanoenergy and Nanosystems, Chinese Academy of Sciences, Beijing 100083, China

[b] Beijing Institute of Basic Medical Sciences, Beijing 100850, China

[c] School of Nanoscience and Technology, University of Chinese Academy of Sciences, Beijing 100049, China

[d] Center on Nanoenergy Research, School of Physical Science and Technology, Guangxi University, Nanning 530004, China

[e] School of Physics, University of Electronic Science and Technology of China, Chengdu 610054, China

[f] School of Physical Education, Jianghan University, Wuhan 430056, China

Corresponding authors: yxwu@jhun.edu.cn (Y. Wu); zli@binn.cas.cn (Z. Li)

Abstract

Schottky-contacted sensors have been demonstrated to show high sensitivity and fast response time in various sensing systems. In order to improve their sensing performance, the Schottky barriers height (SBH) at the interface of semiconductor and metal electrode should be adjusted to appropriate range to avoid low output or low sensitivity, which was induced by excessively high or low SBH, respectively. In this work, a simple and effective SBH tuning method by triboelectric generator (TENG) is proposed, the SBH can be effectively lowered by voltage pulses generated by TENG and gradually recover over time after withdrawing the TENG. Through combining the TENG treatment with piezotronic effect, a synergistic effect on lowering SBH was achieved. The change of SBH is increased by 3.8 to 12.8 times, compared with dependent TENG treatment and piezotronic effect, respectively. Furthermore, the recovery time of the TENG-lowered SBH can be greatly shortened from 1.5 h to 40 s by piezotronic effect. This work demonstrated a flexible and feasible SBH tuning method, which can be used to effectively improve the sensitivity of Schottky-contact sensor and sensing system. Our study also shows great potential in broadening the application scenarios of Schottky-contacted electronic devices.

Keywords: ZnO nanowire, Triboelectric nanogenerator, Schottky barrier height, Piezotronic effect, Modulation

1. Introduction

Semiconductor nano/micro wires (NMWs) have wide applications in electronics[1–3], optoelectronics[4,5], nanoelectromechanics[6,7] and sensing systems[8–10]. ZnO NMWs have high sensitivity in various detections due to their unique electronic/optical properties and large

surface-to-volume ratio such as gas[11], UV light[12] and biochemical molecules[13–15]. Compared with Ohmic contact, Schottky contact is preferred to be formed in ZnO NMW-based sensors for its sensitive current tuning effect [13, 16]. The sensing performance of Schottky-contact sensors mainly relies on the local Schottky barrier height (SBH), which is highly susceptible to the adsorbed charged/polar species on NMW surface.

The SBH at the interface of ZnO NMWs and metal electrode should be modulated to improve the sensitivity of Schottky-contact sensor. On one hand, a too high SBH leads to the rather low output current signal, and a too low SBH will make the sensor's performance be approximate to Ohmic-contact [15]. On the other hand, SBH can be increased by negatively charged molecules and decreased by positively charged molecules [14, 15], to enlarge the concentration range of charged molecules detection, SBH also should be adjusted to suitable value to ensure sufficient variation range.

Many efforts have been made to tune the SBH [16], such as electron beam lithography (EBL) [17], focused ion beam (FIB) [18] and surface modification [19]. These methods are usually technically sophisticated, high-cost and irreversible. According to previous reports in past decades, SBH at ZnO-metal Schottky junction can be dynamically changed in many ways, including piezoelectric effect [20–22], photoexcitation effects [23] and light-self-induced pyroelectric effect [24], these effects especially piezoelectric effect are widely used in detecting various objects with enhanced sensing performance [25–28]. Furthermore, researchers have also demonstrated that comprehensive effect of these effects such as piezo-phototronic effect[29], pyro-phototronic effect[30] can effectively tune SBH and be used to optimize the sensing performance of ZnO NMW based Schottky contact sensors[29–31]

Last year, we proposed an effective SBH regulation method via triboelectric nanogenerators (TENGs) treatment, and demonstrated its feasibility for enhancing sensitivity of ZnO NMW based sensor in various sensing systems [32–34]. SBH of the ZnO NMW-based device can be effectively lowered by the voltage pulses generated from TENG and gradually recover with time after withdrawing the TENG's voltage. During the progress of optimizing this SBH modulation effect, methods were developed to shorten the recovery time of TENG lowered SBH, and we found that the recovery time can be shortened by coupling negative piezopotential. Along this train of thought, we systematically investigated the coupling effect of TENG treatment and piezopotential on SBH and electrical transport characteristics of ZnO NMW devices, and the feasibility of this coupling effect in optimizing the SBH modulation method was successfully proved. Compared with any single treatment effect, the coupling effect achieved a synergistic effect in lowering SBH. Additionally, the compressive strain-induced negative piezopotential can speed up the recovery rate of TENG treated SBHs. This work demonstrated a simple and flexible method of tuning SBH of ZnO NMW-based device by TENG treatment and systematically studied its combination with piezotronic effect, which contributes to achieving more sensitive detection of relevant species and broadening potential applications of Schottky barrier-based electronic devices [35–37].

2. Experimental

2.1 Fabrication of the ZnO NMW-based device

The ZnO NMWs used in this work were synthesized by reported vapor-liquid-solid process [38, 39]. The NMWs were several hundred micrometers long and a dozen micrometers in diameter (Fig. S1 online). The ZnO NMW-based device was fabricated by fixing both ends of a ZnO NMW on the glass substrate (0.5 cm×2.5 cm) with silver paste. Thin layers of epoxy covered on

the sliver electrodes serve as water-proof layer, which can further increase the stability of the electrodes by preventing oxidization in air. The photograph and optical microscope images of the ZnO NMW-based devices and NMWs are shown in the insets in Fig. 1c.

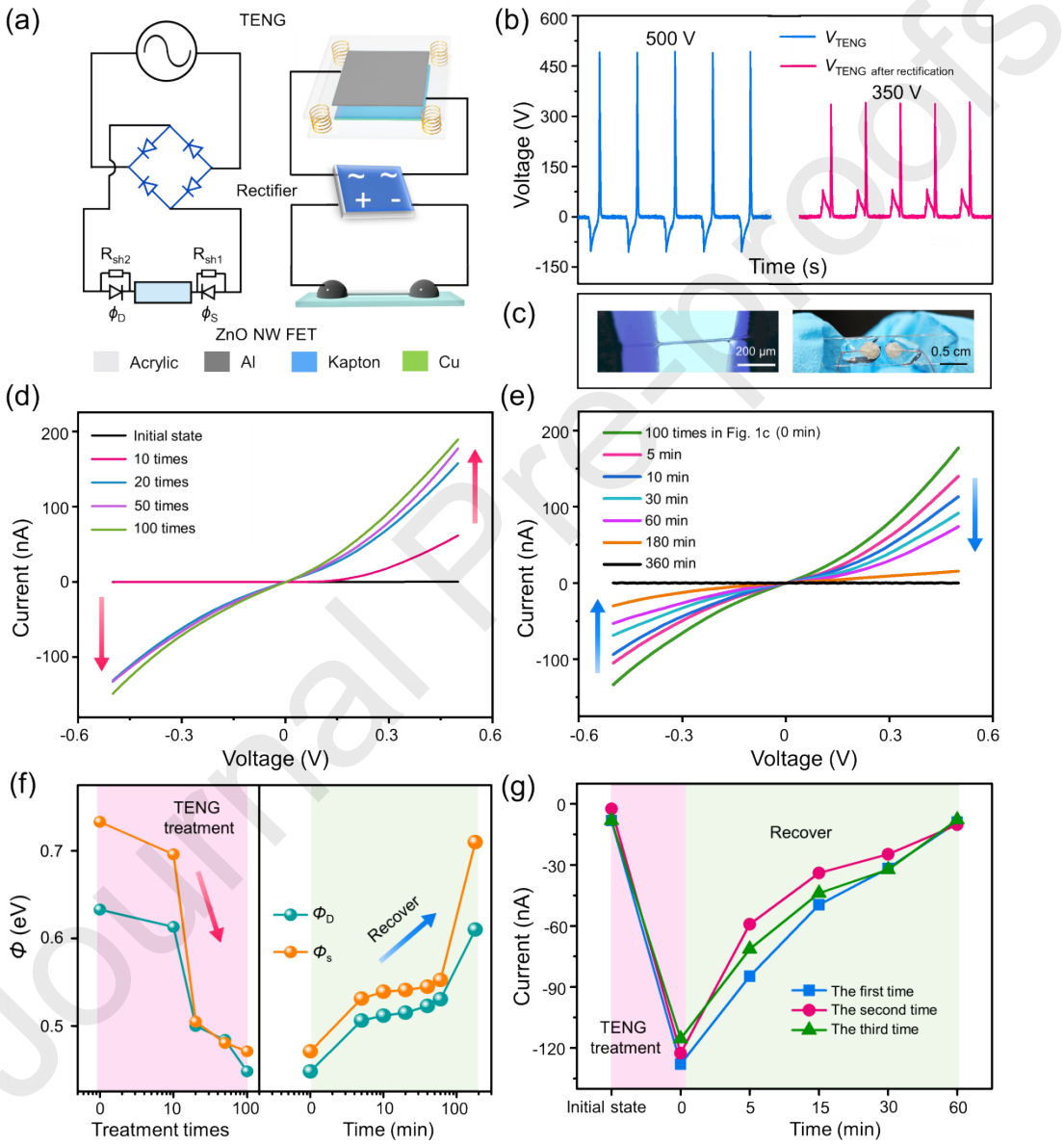

Fig. 1. Tuning SBH of ZnO NMW-based device by TENG. (a) The left and right diagrams represent the equivalent circuit and experiment setup of the ZnO NMW-based device treated by

TENG, respectively. (b) The output voltage of the TENG before (blue) and after rectification (red). (c) The optical images of the ZnO NMW-based device with different magnifications. (d) Current-voltage (*I-V*) curves of the ZnO NMW-based device after different times of TENG treatment. (e) *I-V* recovery curves of ZnO NMW-based device after withdrawing voltage pulses generated by TENG. (f) The SBHs of drain and source as a function of the TENG treatment times and the recovery time. (g) Repeatability of the TENG treatment method, output current at a fixed bias voltage of –2 V in Fig. S3a–c (online) during the 3 repetitions.

2.2 Fabrication of the TENGs with different output voltages

TENGs with different output voltages are fabricated by changing the friction surface. The tribolayers of TENGs were composed of Al foils and Kapton films with a vertical contact-separation mode. Al foils and Kapton films were cleaned with alcohol and cut into uniform-sized pieces (3 cm × 3 cm × 100 μm, 8 cm × 8 cm × 100 μm, 20 cm × 20 cm × 100 μm). Both tribo-surfaces were polished with sandpapers (3000#) in the same direction for 2 times to produce micro structures and increase the friction area. A thin layer of copper film (50 nm) was deposited on Kapton film by magnetron sputtering to serve as back electrode. Copper wires were connected to Al and Cu electrodes by sliver paste. Friction materials were attached on two acrylic plates (10 cm × 10 cm × 4 mm), which are kept parallel with by springs in four corners.

2.3 Coupling effect of the TENG treatment and piezotronic effect

When study the coupling effect of TENG treatment and piezotronic effect, flexible polycarbonate (PC) substrates were used to replace glass substrate to support the ZnO NMW device. The experimental setup is shown in Fig. S2 (online). One end of the device was fasten to a manipulation holder, with the other end free. Compressive or tensile strains were introduced by

bending the free end of the device with a three-dimensional (3D) mechanical stage. The magnitude of stains can be calculated according to Yang et al.'s work [39]. The movement step resolution of the 3D mechanical stage is 1 μm.

3. Result and discussion

3.1 Tuning SBH by TENG.

The ZnO NMW-based device was treated by the rectified voltage pulses generated by TENG (Fig. 1a). In this work, the ZnO NMW-based device was fabricated by fixing both ends of the ZnO NMW on the glass/PC substrate by Ag pastes. The optical images of the ZnO NMW and the fabricated ZnO NMW-based device were shown in Fig. 1c and Fig. S1 (online), the distance between source and drain is about 600 μm. The output voltages of the TENG before and after rectification are 500 V (blue waveform in Fig. 1b) and 350 V (red waveform in Fig. 1b), respectively. The voltage drop after rectification can be attributed to energy loss during the rectification process and the high internal resistance of TENG. Similarly, due to the resistance of ZnO NMW-based device (about 2.7 MΩ) is much smaller than the resistance of TENG (about 50 MΩ), the voltage applied on the ZnO NMW-based device is only about 18 V, which is much smaller than the rectified voltage (i.e., 350 V) (Fig. S3 online). The current generated from TENG also decreases after rectification, and the current applied on the ZnO NMW-based device is a little smaller than the current after rectification (Fig. S4 online).

Typical *I-V* curves after different times of TENG treatment are shown in Fig. 1d. The *I-V* curves shift upwards obviously with TENG treatment times (Fig. 1d), and then gradually shift downward with time after withdrawing the voltage pulses generated by TENG (Fig. 1e). The shape of *I-V* curve depends on the SBH formed between metal (Ag) and semiconductor (ZnO)

because of different interface properties [21, 40]. For the SBHs of source and drain, the values decrease from 0.73 to 0.47 eV and 0.63 to 0.45 eV after 100 times of TENG treatment, respectively (Fig. 1f). Then the values increased to 0.71 and 0.61 eV, respectively, after withdrawing the voltage pulses generated by TENG for 6 h (Fig. 1f). To prove the repeatability of this method, the process of 50 times of TENG treatment is repeated for 3 times. The characteristics of *I-V* curve and SBHs show the same variation trend (Fig. S5 online and Fig. 1g). Based on these results, it is reasonable to conclude that the SBHs of the ZnO NMW-based device can be lowered by the TENG treatment and gradually recovered with the time increasing after withdrawing the TENG voltage pulses.

Three TENGs with different out voltages (100, 500, 1000 V) were fabricated to investigate the relationship between the applied voltage and SBHs. The three TENGs are named TENG A (100 V), TENG B (500 V) and TENG C (1000 V), respectively (Fig. 2a). After rectification, the output voltage of these three TENGs are 80, 350 and 850 V (Fig. 2b), respectively. The voltages applied on the ZnO NMW-based device are 7, 19 and 32 V (Fig. S6 online), respectively.

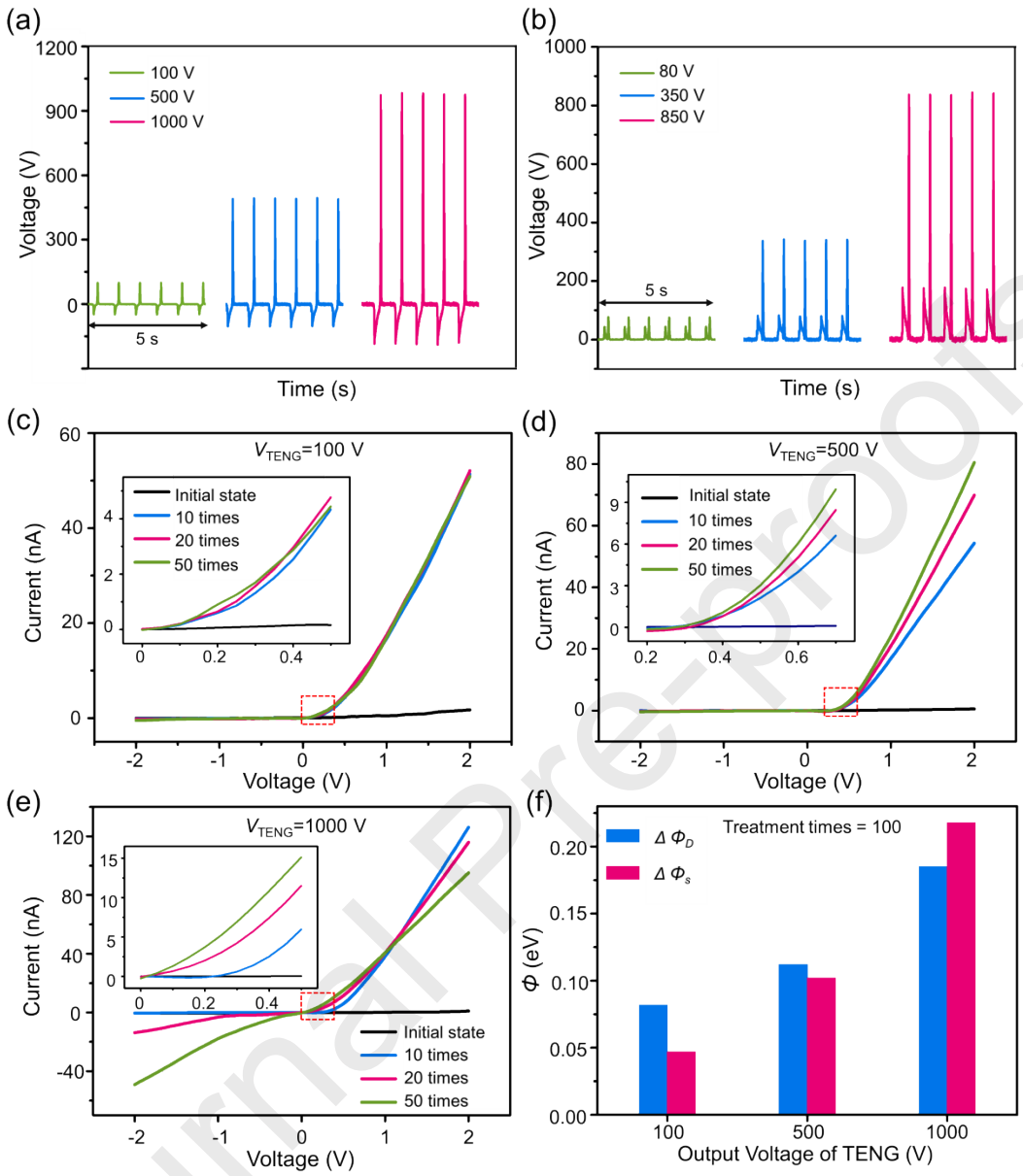

Fig. 2. Tuning SBH of ZnO NMW-based device by TENG with different voltage. (a) Open-circuit voltages of the three TENGs. (b) Open-circuit voltage waveforms of the 3 TENGs after rectification. (c–e) *I-V* characteristics of the ZnO NMW-based FET after it was treated with three TENGs with different times, the output voltage of three TENGs are 100, 500, and 1000 V, respectively. Insets in Fig. 2c–e are the enlarged *I-V* curves to present more details. (f)

Comparison of lowered SBHs at the drain and source electrodes after treated by three TENGs (100, 500, 1000 V) for the same number of times (100).

Fig. 2c shows the *I-V* curves of the ZnO NMW device after treated by TENG A (100 V) for different times. After 50 times of treatment, the output current at 2 V increases from 2 to 52 nA. SBHs at the drain and source electrodes decrease from 0.665 and 0.70 eV to 0.627 and 0.635 eV (Fig. S7a online), respectively. When the number of TENG treatment times exceeds 10, the *I-V* curves in Fig. 2c are almost overlapped (the inset in Fig. 2c), which indicates the lowering effect is almost saturated for the TENG A at this voltage (100 V).

Fig. 2d and e show the *I-V* curve change after treated by TENG B (500 V) and TENG C (1000 V), respectively. After treated for 50 times by TENG B, the output current at +2 V increases from 2 to 80 nA (Fig. 2d). With the continued increasing of the number of TENG treatment times, the output current at +2 V increases to 120 nA after 4000 times of TENG B treatment, and the *I-V* curves corresponding to 4000 and 8000 times are also almost overlapped, which is similar with the saturated SBH lowering effect in the case of TENG A (Fig. S8 online). In the case of TENG C, the current at +2 V increases from 2 to 126 nA after only 10 times of treatment which is higher than 120 nA (i.e., the maximum output current at +2 V in the case of TENG B). Similarly, in Fig. 2c, d and Fig. S8 (online), the range of current responses in negative bias (–2–0 V) is too small and seems almost unchanged compare with that in Fig. 2e. As shown in Fig. S9 (online, the enlarged *I-V* curves in negative bias in Fig. 2c and d.), the output current at –2 V also increases with TENG treatment times but changes within the scope of 1 nA. While it can be increased from –1 to –40 nA after treated for 50 times by TENG C (1000 V), the rectification characteristic of the ZnO NMW device vanished, this reconfirms that the current

increase is more noticeable at a high voltage. The comparison of lowered SBHs also shows that TENG with higher voltage has more remarkable SBH lowering effect (Fig. 2f).

3.2 Mechanism explanation of SBH variation.

Researchers have studied the driving and producing processes of oxygen vacancies in the past decades [41–45]. According to previous works, during the preparation of ZnO nanowire, the native defects of oxygen vacancies are generated in ZnO inevitably [42]. An oxygen vacancy can in principle take on different valence states (V_O^{2+}, V_O^{+} and V_O^{0}), the neutral oxygen vacancies (V_O^{0}) at the metal-ZnO interface can be readily converted into an ionized oxygen vacancy (V_O^{2+}) [43,44]. The formation of Schottky junction appears to be strongly influenced by the density of oxygen vacancies (V_O) near the metal-ZnO interface [43]. The high electric field could exert the force on positively charged oxygen vacancies in the direction of the interface and initiate ion migration [45]. In this work, positively charged oxygen vacancies (V_O^{2+}) can be driven by the voltage pulses generated by TENG. The ionized oxygen vacancies (V_O^{2+}) accumulated at ZnO-Ag interface create a narrow region of positive space charge close to the interface which can bend the energy band at ZnO-Ag interface and reduce SBH [43].

Therefore, the physical process of ionized oxygen vacancies being driven to accumulate at the metal-semiconductor (M-S) interface after the device is treated by the voltage pulses of TENG can be illuminated by the classical polarization model. The schematic diagram of SBH variation process is shown in Fig. 3. In the initial state, Ag paste and one end of n-type ZnO NMW formed Schottky contact, a Schottky barrier is created at the interface, the schematic atomic structure and energy-band diagram of the interface is shown in Fig. 3a. After different times of TENG treatment, the positive charged oxygen vacancies accumulate at the M-S interface, the increased density of ionized oxygen vacancy near ZnO-Ag interface leads to SBH

decrease, as shown in Fig. 3b. After withdrawing the voltage pulses generated by TENG, the oxygen vacancies diffuse away from ZnO-Ag interface and move deeper into ZnO due to unbalanced distribution of oxygen caused by the external electric field [45]. Concentration of oxygen vacancies near ZnO-Ag interface begins to decrease, which results in SBH recovery (Fig. 3c).

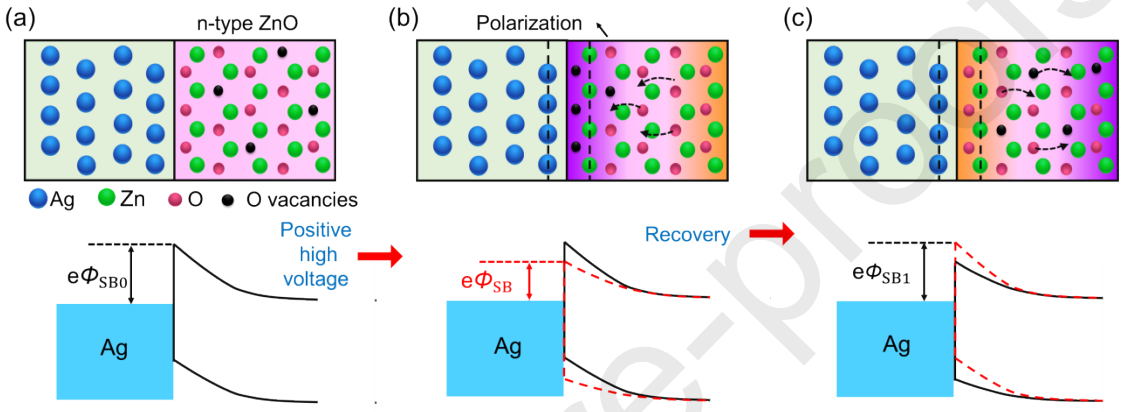

Fig. 3. Polarization model and SBH variation diagram. (a) The model of an M-S contact consisted of Ag and n-type ZnO with Schottky contact. The initial SBH is Φ_{SB0}. (b) The positively charged oxygen vacancies (V_O^{2+}) are driven by positive high voltage pulses of TENG to diffuse to ZnO-Ag interface, the positively charged oxygen vacancies (V_O^{2+}) accumulated at interface result in the bend of energy band and SBH decrease (from Φ_{SB0} to Φ_{SB}). (c) The ionized oxygen vacancies diffuse away from ZnO-Ag interface slowly after withdrawing the treatment of positive high voltage of TENG, the density of positively charged oxygen vacancies (V_O^{2+}) decrease which results in SBH increase to Φ_{SB1}.

Within a certain range of TENG times, the density of ionized oxygen vacancy near ZnO-Ag interface increases with TENG treatment times, so SBH at Schottky junction decreases with the

increasing times of TENG. Due to the vacancies at low electric field region move more slowly compared to the ones at high electric field region [45]. Therefore, sufficiently strong electric field can induce an ionized oxygen vacancy concentration buildup at the Schottky junction interface, which leads to the change of the effective SBH. This could explain why TENG with higher voltage has more remarkable effect of lowering SBH. After certain times of TENG treatment, the migration of oxygen vacancies to ZnO-Ag interface induced by TENG treatment and the diffusion of vacancies away from ZnO-Ag interface reach to a balanced state, SBH no longer changes obviously with the increase in TENG treatment times, which leads to *I-V* curves overlapped in responses.

Various M-S contact behaviors can result in distinctly different *I-V* curves at M-S interfaces [39]. Besides, it has been reported that SBH at both ends of the ZnO NMW device can be lowered after the device is under the strong electric field[46]. We have also verified that SBHs of drain and source both decreased with TENG treatment times whatever the direction of voltage pulses generated by TENG (Fig. S10 online). For simplicity, an ideal classic M-S-M model with one perfect end is adopted, in this case, the electric property of the device mainly depends on the forward voltage [47]. In this research, the characteristic change of one interface after the device is treated by the voltage pulses of TENG can be demonstrated by this simplified model qualitatively.

For a one-dimensional model, the built-in potential φ_{bi} is given by [47–49]

$$\varphi_{\mathrm{bi}} = \frac{q}{2\varepsilon_{\mathrm{s}}}\left(N_{\mathrm{A}}W_{\mathrm{Dp}}^2 + \rho_{\mathrm{polar}}W_{\mathrm{polar}}^2 + N_{\mathrm{D}}W_{\mathrm{Dn}}^2\right) \quad , \quad (1)$$

Where ε_{s} is the permittivity of the material, q is the absolute value of the unit electronic charge, N_{D} and N_{A} are the donor and acceptor concentration, respectively. In addition, ρ_{polar} is the polarization charges density and W_{polar} is the distribution width of oxygen vacancies, ρ_{polar} and

W_{polar} are function of time that are gradually build up when the TENG bias is applied. The W_{Dp} and W_{Dn} are the widths of depletion region on the p-type and n-type, respectively. Because the ZnO NMW used in this work is n-type, the N_A and W_{Dp} can be assumed to be zero in this study. Current-voltage characteristics of the M-S junction is given by [48]

$$J = J_0 \exp\left(\frac{q^2 \rho_{polar} W_{polar}^2}{2\varepsilon_s kT}\right)\left[\exp\left(\frac{qV}{kT}\right) - 1\right] \quad , \quad (2)$$

where V is the bias voltage, k_B is the Boltzmann constant and T is the temperature, J_0 is the saturation current density. For M-S contact, J_0 is given by [48]

$$J_0 = \frac{q^2 D_n N_c}{kT}\sqrt{\frac{2qN_D(\varphi_{bi0} - V)}{\varepsilon_s}}\exp\left(-\frac{q\Phi_{SB0}}{kT}\right) \quad , \quad (3)$$

where N_c is the effective density of states at conduction band, D_n is electron diffusion coefficients, Φ_{SB0} is the Schottky barrier height and φ_{bi0} is the built-in potential without polarization charges. Many previous studies have investigated the influence about polarization charges to SBH. Therefore, after polarization, the initial SBH (Φ_{SB0}) of one dimensional M-S model can be decreased to Φ_{SB} [48]

$$\Phi_{SB} = \Phi_{SB0} - \frac{q\rho_{polar} W_{polar}^2}{2\varepsilon_s} \quad . \quad (4)$$

3.3 Coupling effect of the TENG treatment and piezotronic effect

From above results, it is well proved that the TENG treatment can effectively lower the SBHs of ZnO NMW-based device. Besides voltage pulses generated from TENG, SBH can also be effectively lowered by DC electrical pulses and DC constant voltage (Fig. S11 online). Compare with DC constant voltage, voltage pulses result in low energy applied on ZnO NMW devices over the same period, the way of electric pulse is chosen to protect ZnO NMW devices. Compare with other electric pulse power sources, TENG has the advantage of easy fabrication,

low cost, environmentally-friendly and superior security due to its features of high voltage and low current.

To further optimize this SBH modulation method by TENG, another strategy (i.e., piezotronic effect) is introduced to study the coupling effect of the two SBH modulation methods. Piezotronic effect has been widely used to tune SBHs of ZnO NMW-based device by compressive or tensile strain due to the wurtzite structure of ZnO [50]. In the following parts, coupling effect of TENG treatment and piezopotential induced by compressive/tensile strains on SBH modulation was systematically researched in Figs. 4–6.

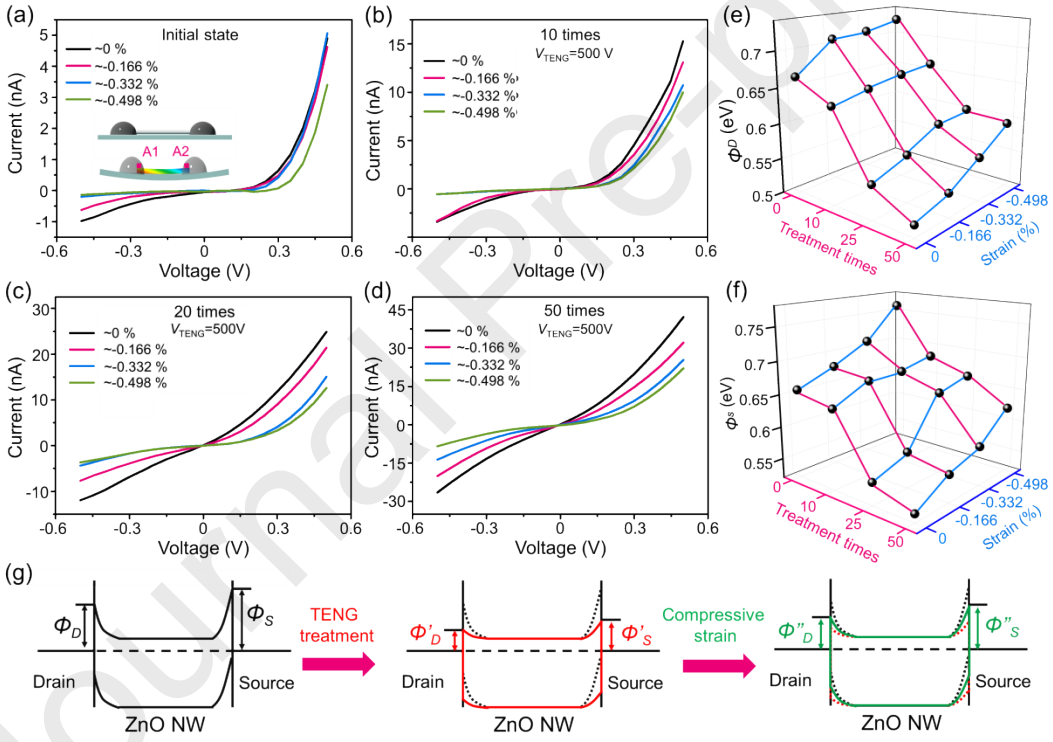

Fig. 4. Coupling effect of the TENG treatment and piezotronic effect induced by compressive strains. (a) *I-V* curves of the ZnO NMW-based device at different compressive strains. The inset schematically shows the ZnO NMW-based device under compressive straining condition. (b–d) *I-V* curves of the ZnO NMW-based device at different compressive strains after treated with TENG for (b) 10 times, (c) 25 times and (d) 50 times. (e, f) 3D graphs of SBHs response to

compressive strain and TENG treatment times. (g) Energy band diagrams of ZnO NMW-based device in the initial state (black lines in (g)), treated by TENG (red lines in (g)), treated by TENG and compressively strained (green lines in (g)), respectively.

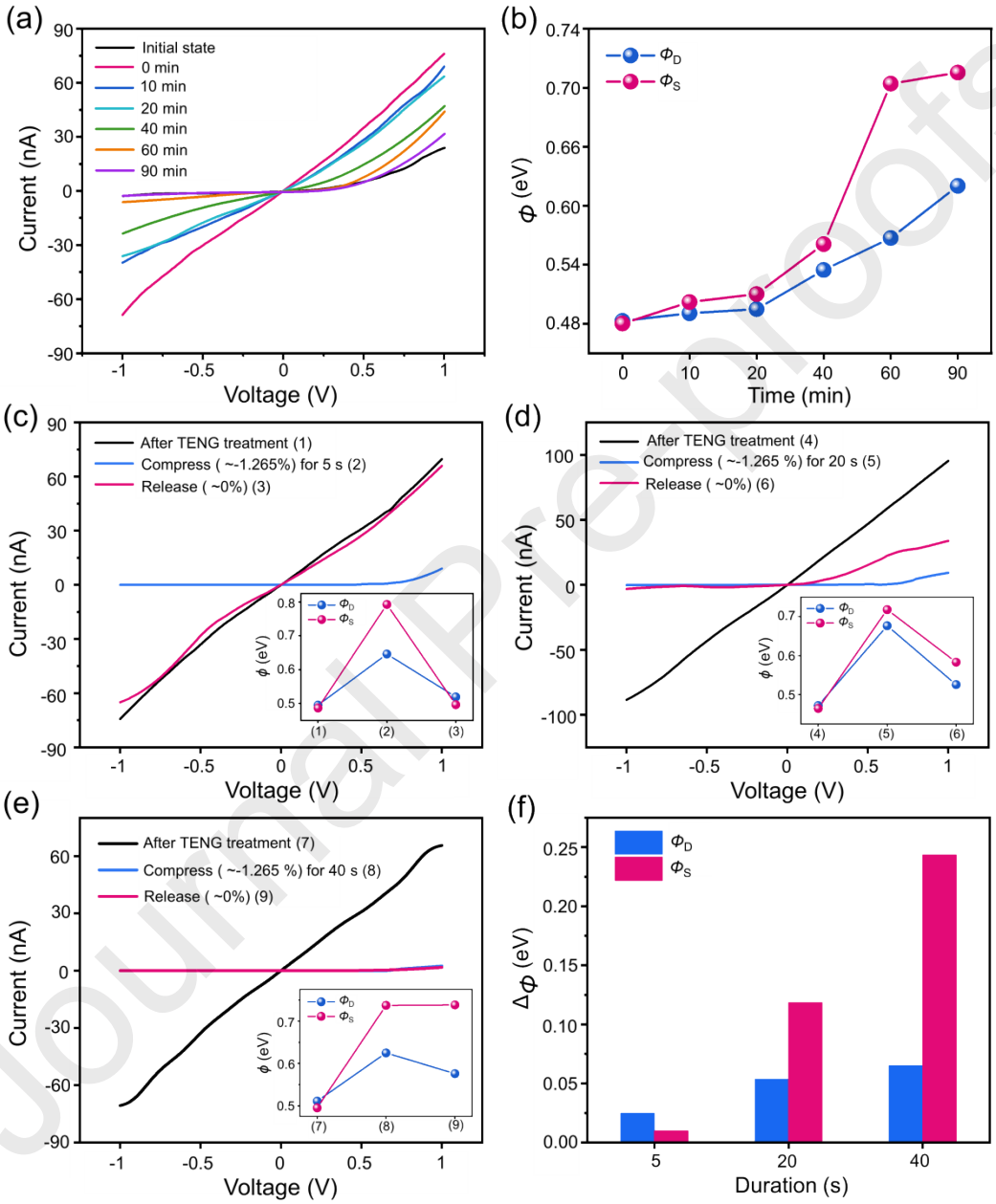

Fig. 5. Compressive strains induced piezotronic effect shorten the recovery time of TENG-lowered SBH. (a) *I-V* recovery curves of ZnO NMW-based device after withdrawing TENG. (b)

The SBHs of drain and source as a function of the recovery time in Fig. 5a. (c–e) *I-V* curves and corresponding SBHs at the compressive strain of –1.265% for 5, 20 and 40 s after TENG treatment. (f) Comparison of SBH variations at the drain and source electrodes after applying compressive strain of –1.265% to the ZnO NMW-based device for different durations (5, 20 and 40 s).

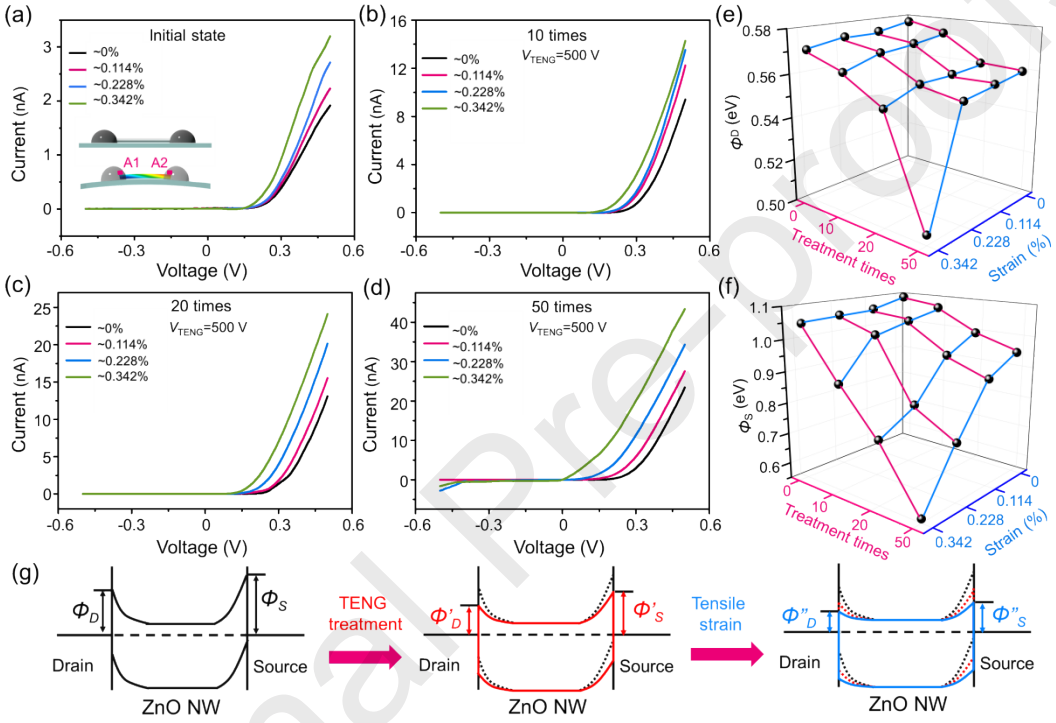

Fig. 6. Coupling effect of the TENG treatment and piezotronic effect induced by tensile strain. (a) *I-V* curves of the ZnO NMW-based device at different tensile strains without TENG treatment. The inset schematically shows the ZnO NMW-based device under tensile straining condition. (b–d) *I-V* curves of the ZnO NMW-based device at different tensile strains after TENG treatment for (b) 10 times, (c) 25 times and (d) 50 times. (e, f) 3D graphs of the SBHs response of drain and source to tensile strain and TENG treatment times. (g) Energy band diagrams of ZnO NMW-based device in the initial state (black lines in (e)), treated by TENG (red lines in (e)) and treated by combination of TENG and tensile strain (blue lines in (e)).

As shown in Fig. 4a–d, four groups of *I-V* curves illustrate the piezotronic effect (compressive strain) on the performance of ZnO NMW-based device before and after different times of TENG treatment (0 time, 10 times, 25 times and 50 times). Fig. 4a shows how the piezotronic effect induced by compressive strain independently tune the performance of the ZnO NMW-based device. It is obvious that the output current in the range of –0.5 and + 0.5 V decreases as the applied compressive strain increases from 0% to –0.498%. The SBHs of source and drain computed from the *I-V* curves increase as the compressive strain increases (Fig. S12a online). As the TENG treatment times increases, the *I-V* curves over the entire voltage range shift upwards, and the SBHs decreases as mentioned above (Fig. S13a, b online) [39]. After combined the compressive strain with TENG treatment for different times, similar trends are observed from the other three groups of *I-V* curves in Fig. 4b–d. The *I-V* curves show higher current response to the bias voltage from –0.5 to +0.5 V compared with the independent piezotronic effect. These results indicate that the piezotronic effect by compressive strain can be successfully combined with TENG treatment.

To further demonstrate the combination effect, the current response to two fixed voltages of –0.5 and +0.5 V were tested and plotted by a 3D scatter plots in Fig. S13c and d (online), respectively. The currents monotonically decrease with increasing compressive strain at a fixed TENG treatment time and increases with the increasing TENG treatment times at a fixed compressive strain. The varying trend for different applied compressive strains is more remarkable after TENG treatment. The SBHs of drain and source as a function of TENG treatment times and compressive strains are plotted as two 3D scatter graphs in Fig. 4e, f. SBHs at both ends monotonically decreases with the increasing TENG treatment times at a fixed

compressive strain and increases with increasing compressive strain at a fixed TENG treatment times.

In order to explain coupling effect of TENG treatment and piezotronic effect induced by compressive strain, a theoretical model of a ZnO NMW-based device is proposed using energy band diagram (Fig. 4g). The energy band structure of a strain free ZnO NMW device before TENG treatment is shown in the left diagram in Fig. 4g. After TENG treatment, SBHs at both ends decrease as we explained previously (the middle diagram in Fig. 4g). The ZnO NMW-based device used in this work is the top electrode configuration [46, 51], the electrical contact areas formed between Ag electrodes and the two ends of the ZnO NMW are named A1 and A2 (inset in Fig. 4a), respectively. When the compressive strain is applied to the device, the induced piezopotential at positions A1 and A2 decreases with the increasing compressive strain. The decrease of negative piezopotential at positions A1 and A2 would lead to increase in SBHs of source and drain and decrease in the current response to bias voltage (the right diagram in Fig. 4g).

TENG treatment can lower SBHs at both ends of the ZnO NMW-based device effectively, however, the recovery time of TENG-lowered SBH is long, which ranges from tens of minutes or even several hours. In Fig. 5a, after withdrawing the voltage pulses generated by TENG, it takes about 90 min for the ZnO NMW device to recover to the approximately original state. This is because the positively charged oxygen vacancies accumulated at ZnO-Ag interface slowly diffuse away from ZnO-Ag interface and move deeper into ZnO, the concentration of oxygen vacancies near ZnO-Ag interface decreases slowly, so the SBH at ZnO-Ag interface recover slowly (Fig. 5b). As shown in Fig. S14 (online), the TENG-lowered SBHs can be quickly increased right after the negative potential induced by compressive strains. The negative

piezocharges induced by compressive strain can offset the SBH lowering effect induced by positive charged oxygen vacancies to some extent, which exhibits an alternative and potential method to speed up the recovery rate of TENG treated *I-V* curves.

To research whether the compressive strain-induced piezotronic effect can speed up the recovery rate compared with independent TENG treatment. Different durations (5, 20, 40 s) of compressive strains (~–1.265%) were applied on the ZnO NMW-based device after treated with TENG (Fig. 5c–e). The *I-V* curves before and after applying compressive strains (~–1.265%) for 5 s are nearly unchanged, and TENG-lowered SBHs at drain and source also do not change very much (Fig. 5c). When the duration of compressive strains is 20 s, the *I-V* curves shift downwards and TENG-lowered SBHs at drain and source increased compare with the initial state after the compressive strain was released (Fig. 5d). Once the duration of compressive strains extend to 40 s, the *I-V* curves did not show more changes after the compressive strain was released, and TENG-lowered SBHs at drain and source recovered significantly compare with those in Fig. 5c and d (Fig. 5e). The comparison of lowered SBHs shows that the longer duration of compressive strains, the more SBHs will be covered (Fig. 5f). Additionally, this effect is sustainable after withdrawing the compressive strain. These results indicate that the compressive strain can be an effective means to speed up the recovery rate of TENG treated *I-V* curves and corresponding SBHs, and the recovery time of TENG-lowered SBH can be greatly shortened from 1.5 h to 40 s.

After the combination of compressive strain-induced piezotronic effect and TENG treatment in Fig. 4, the tensile strain-induced piezotronic effect was also combined with TENG treatment in the following Fig. 6. As shown in Fig. 6a–d, four groups of *I-V* curves illustrate the tensile strain-induced piezotronic effect on the performance of ZnO NMW-based device after different times of TENG treatment (0 time, 10 times, 25 times and 50 times). Compare with the

compressive strain-induced piezotronic effect, the tensile strain-induced piezotronic effect improves the current response of the ZnO NMW-based device and lowers the SBHs of source and drain obviously (Fig. 6a–d and Fig. S15a–d online), which has the similar effect with the TENG treatment method (Fig. S16a online). To systematically investigate the coupling effect of TENG treatment and the tensile strain-induced piezotronic effect, the results are extracted from the *I-V* curves (Fig. 6a–d) and plotted in Fig. S16b (online). It is straightforward to see that the current increases with the TENG treatment times at a fixed tensile strain or increases with tensile strain at a fixed TENG treatment times. The change in *I-V* curves indicates that the SBHs at both ends also decrease with the increase of TENG treatment times or tensile strains. The variation trend was plotted by 3D graphs in Fig. 5e and f, the date points were extracted from Fig. S15a–d (online). Comparison of lowered SBHs at the drain and source electrodes after different SBH tuning methods were calculated from Fig. 6e and f and were shown in Fig. S17 (online). Compared with SBH tuning method A (i.e., tensile strain-induced piezotronic effect: tensile strain = 0.342%) and B (i.e., TENG treatment (V_{TENG}=500 V, treatment times=50 times), the combination of method A and B (method A&B) have more significant SBH lowering effect than any single SBH tuning method. The method A&B induces about 11.2-fold and 4.2-fold increase in $\Delta\Phi_D$ (the decreasing amount of Φ_D) compared to method A and method B, respectively; and $\Delta\Phi_S$ (the decreasing amount of Φ_S) is also increased by a factor of 12.8 and 3.8 compared with method A and method B.

Fig. 6g shows the energy band change of the ZnO NMW-based device under tensile strain after TENG treatment. Unlike the compressive strain, the induced piezopotential at positions A1and A2 (Fig. 6a) are positive and increases with the increasing tensile strain, which result in the decrease in SBHs of drain and source. These results show that by combining the TENG

treatment method with tensile strain-induced piezotronic effect, a synergistic effect on lowering SBH and enhancing current response can be achieved compared with any single treatment method.

From Figs. 4 and 6, the piezotronic effect by both compressive and tensile strain can combine with TENG treatment successfully. The compressive strain-induced piezotronic effect raises the SBHs, which will speed up the recovery rate of the TENG-lowered SBH. The tensile strain-induced piezotronic effect lowers the SBH and enhanced the current response of the ZnO NMW-based device further.

4. Conclusion

In summary, we have demonstrated a new and effective SBH tuning method by TENG treatment and its combination with piezotronic effect. The SBHs at ZnO-Ag paste interfaces are decreased by TENG treatment and can gradually recover to their initial state over time after withdrawing the output voltage from TENG. Compared with the lower voltage, a higher TENG voltage has a more remarkable effect of lowering SBH. The change in SBH can be attributed to the migration of ionized oxygen vacancies in ZnO nanowires as driven by external voltage pulses provided by TENG. After combining the TENG treatment with piezotronic effect, a synergistic effect was achieved. The SBH is lowered and current response is increased, among which the change of SBH is improved by a factor of 3.8 to 12.8, comparing with the two dependent treatment methods. Additionally, the piezotronic effect can also greatly shorten the recovery time of SBH, which is lowered by TENG, from 1.5 h to 40 s. This study demonstrates a new method for optimizing SBH modulation, which shows significance in improving the sensitivity and response value of Schottky sensors in detecting UV light, gas and biomolecular species in applications.

Conflict of interest

The authors declare that they have no conflict of interest.

Acknowledgments

This work was supported by the National Key R&D Program of China (2016YFA0202703), Key-Area Research and Development Program of Guangdong Province (2018B030331001), the National Natural Science Foundation of China (61875015, 81971770, 52002027, 82071970), Beijing Natural Science Foundation (JQ20038, 2214083), China National Postdoctoral Program for Innovative Talent (BX20200380), and the Fundamental Research Funds for the Central Universities.

Author contributions

Zhou Li, Luming Zhao, Yuxiang Wu conceived the idea and designed the experiment. Zhou Li, and Yuxiang Wu guided the project. Luming Zhao and Hu Li fabricated the devices, performed the experiment. Luming Zhao and Zhou Li analyzed the data. Yan Zhang developed the theoretical models. Luming Zhao drew the figures. Luming Zhao, Hu Li, Janping Meng. and Hongqing Feng. prepared the manuscript. All authors discussed and reviewed the manuscript.

References:

[1]. Duan X, Huang Y, Agarwal R, et al. Single-nanowire electrically driven lasers. *Nature* **2003;** 421: 241-5.

[2]. Chen C Y, Huang J H, Song J, et al. Anisotropic outputs of a nanogenerator from oblique-aligned ZnO nanowire arrays. *ACS Nano* **2011;** 5: 6707-13.

[3]. Xue J, Song J, Dong Y, et al. Nanowire-based transparent conductors for flexible electronics and optoelectronics. *Sci Bull* **2017;** 62: 143-56.

[4]. Huang Y, Cheng K, Liu J, et al. Size dependence of photovoltaic properties and surface states modulation in ZnO nanowire/poly(3-hexylthiophene) hybrid nanostructures. *Sci Bull* **2016;** 61: 245-51.

[5]. Liu S, Liao Q, Lu S, et al. Strain modulation in graphene/ZnO nanorod film Schottky junction for enhanced photosensing performance. *Adv Funct Mater* **2016;** 26: 1347-53.

[6]. Wu W, Wang Z L. Piezotronic nanowire-based resistive switches as programmable electromechanical memories. *Nano Lett* **2011;** 11: 2779-85.

[7]. Sazonova V, Yaish Y, Üstünel H, et al. A tunable carbon nanotube electromechanical oscillator. *Nature* **2004;** 431: 284-7.

[8]. Patolsky F, Timko B P, Yu G H, et al. Detection, stimulation, and inhibition of neuronal signals with high-density nanowire transistor arrays. *Science* **2006;** 313: 1100-04.

[9]. Zhou W, Dai X, Lieber C M. Advances in nanowire bioelectronics. *Rep Prog Phys* **2016;** 80: 016701.

[10]. Menzel A, Subannajui K, Güder F, et al. Multifunctional ZnO-nanowire-based sensor. *Adv Funct Mater* **2011;** 21: 4342-48.

[11]. Wei T Y, Yeh P H, Lu S Y, et al. Gigantic enhancement in sensitivity using Schottky contacted nanowire nanosensor. *J Am Chem Soc* **2009;** 131: 17690-95.

[12]. Zhou J, Gu Y, Hu Y, et al. Gigantic enhancement in response and reset time of ZnO UV nanosensor by utilizing Schottky contact and surface functionalization. *Appl Phys Lett* **2009;** 94: 191103.

[13]. Yeh P H, Li Z, Wang Z L. Schottky-gated probe-free ZnO nanowire biosensor. *Adv Mater* **2010:** 21: 4975-78.

[14]. Hu Y, Zhou J, Yeh P H, et al. Supersensitive, fast-response nanowire sensors by using Schottky contacts. *Cheminform* **2010:** 22: 3327-32.

[15]. Yu R, Pan C, Chen J, et al. Enhanced performance of a ZnO nanowire-based self-powered glucose sensor by piezotronic effect. *Adv Fun. Mater* **2013;** 23: 5868-74.

[16]. Cox J W, Foster G M, Jarjour, A; et al. Defect manipulation to control ZnO micro-/nanowire-metal contacts. *Nano Lett* **2018;** 18: 6974-80.

[17]. Moretto L, Tormen M, De Leo M, et al. Polycarbonate-based ordered arrays of electrochemical nanoelectrodes obtained by e-beam lithography. *Nanotechnology* **2011;** 22: 185305.

[18]. Han G, Weber D, Neubrech F, et al. Infrared spectroscopic and electron microscopic characterization of gold nanogap structure fabricated by focused ion beam. *Nanotechnology* **2011;** 22: 275202.

[19]. Lao C, Li Y, Wong C, et al. Enhancing the electrical and optoelectronic performance of nanobelt devices by molecular surface functionalization. *Nano Lett* **2007;** 7: 1323-28.

[20]. Wang, Z. L. Progress in piezotronics and piezo-phototronics. *Adv Mater* **2012,** 24, (34), 4632-4646.

[21]. Zhou J, Fei P, Gu Y, et al. Piezoelectric-potential-controlled polarity-reversible Schottky diodes and switches of ZnO wires. *Nano Lett* **2008;** 8: 3973-77.

[22]. Fei P, Yeh P H, Zhou J, et al. Piezoelectric potential gated field-effect transistor based on a free-standing ZnO wire. *Nano Lett* **2009;** 9: 3435-39.

[23]. Hu Y, Chang Y, Fei P, et al. Designing the electric transport characteristics of ZnO micro/nanowire devices by coupling piezoelectric and photoexcitation effects. *ACS Nano*, **2010**, 4: 1234-40.

[24]. Wang Z, Yu R, Pan C, et al. Light-induced pyroelectric effect as an effective approach for ultrafast ultraviolet nanosensing. *Nat. Commun*, **2015**, 6: 8401.

[25]. Zhou R, Hu G, Yu R, et al. Piezotronic effect enhanced detection of flammable/toxic gases by ZnO micro/nanowire sensors. *Nano Energy* **2015;** 12: 588-96.

[26]. Yang Q, Guo X, Wang W, et al. Enhancing sensitivity of a single ZnO micro-/nanowire photodetector by piezo-phototronic effect. *ACS Nano* **2010;** 4: 6285-91.

[27]. Yu R, Pan C, Wang Z L. High performance of ZnO nanowire protein sensors enhanced by the piezotronic effect. *Energy Environ Sci* **2013;** 6: 494-99.

[28]. Yu R, Niu S, Pan C, et al. Piezotronic effect enhanced performance of Schottky-contacted optical, gas, chemical and biological nanosensors. *Nano Energy* **2015;** 14: 312-39.

[29]. Yang Q, Guo X, Wang W, et al. Enhancing sensitivity of a single ZnO micro-/nanowire photodetector by piezo-phototronic effect. *ACS Nano*, **2010**, 4: 6285-91.

[30]. Wang Y, Zhu L, Feng Y, et al. Comprehensive pyro-phototronic effect enhanced ultraviolet detector with ZnO/Ag Schottky junction. *Adv Funct Mater*, **2019**, 29: 1807111.

[31]. Wang P, Fu Y, Yu B, et al. Realizing room-temperature self-powered ethanol sensing of ZnO nanowire arrays by combining their piezoelectric, photoelectric and gas sensing characteristics. *J Mater Chem A*, **2015**, 3: 3529-35.

[32] Meng J, Li H, Zhao L, et al. Triboelectric nanogenerator enhanced Schottky nanowire sensor for highly sensitive ethanol detection. *Nano Lett* **2020;** 20: 4968-74.

[33]. Li H, Zhao L, Meng J, et al. Triboelectric-polarization-enhanced high sensitive ZnO UV sensor. *Nano Today* **2020**; 33:100873.

[34]. Zhao L, Li H, Meng J, et al. Reversible conversion between Schottky and Ohmic contacts for highly sensitive, multifunctional biosensors. *Adv Funct Mater* **2020**; 30: 1907999.

[35]. Zhu M, Sun Z, Zhang Z, et al. Haptic-feedback smart glove as a creative human-machine interface (HMI) for virtual/augmented reality applications. *Sci Adv*, **2020**, 6: eaaz8693.

[36]. Garcia-Basteiro AL, Moncunill G, Tortajada M, et al. Seroprevalence of antibodies against SARS-CoV-2 among health care workers in a large Spanish reference hospital. *Nat Commun*, **2020**, 11: 3500.

[37]. Meng J, Li Z. Schottky-contacted nanowire sensors. *Adv Mater* **2020**, 32, 2000130.

[38]. Wang X, Summers C J, Wang Z L. Large-scale hexagonal-patterned growth of aligned ZnO nanorods for nano-optoelectronics and nanosensor arrays. *Nano Lett* **2004;** 4: 423-6.

[39]. Zhou J, Gu Y, Fei P, et al. Flexible piezotronic strain sensor. *Nano Lett* **2008;** 8: 3035-40.

[40]. Liu Y, Kauser M Z, Nathan M I, et al. Effects of hydrostatic and uniaxial stress on the Schottky barrier heights of Ga-polarity and N-polarity n-GaN. *Appl Phys Lett* **2004;** 84: 2112-14.

[41]. Ding Y, Liu Y, Niu S, et al. Pyroelectric-field driven defects diffusion along c-axis in ZnO nanobelts under high-energy electron beam irradiation *J Appl Phys* **2014;** 116: 154304.

[42] Janotti, A; Van de Walle, C G. Native point defects in ZnO. *Phys Rev B: Condens Matter Mater Phys* **2007**, 76, 165202.

[43] Allen MW, Durbin SM. Influence of oxygen vacancies on Schottky contacts to ZnO. *Appl Phys Lett*, **2008**, 92:122110.

[44] Min Y. Properties and sensor performance of zinc oxide thin films. Doctor Dissertation. Massachusetts Institute of Technology, **2003**.

[45] Jiang W, Noman M, Lu Y M, et al. Mobility of oxygen vacancy in $SrTiO_3$ and its implications for oxygen-migration-based resistance switching. *J Appl Phys*, **2011**, 110: 034509.

[46]. Xue F, Zhang L, Feng X, et al. Influence of external electric field on piezotronic effect in ZnO nanowires. *Nano Res* **2015;** 8: 2390-99.

[47]. Zhang Z, Yao K, Liu Y, et al. Quantitative analysis of current-voltage characteristics of semiconducting nanowires: decoupling of contact effects. *Adv Funct Mater* **2007;** 17: 2478-89.

[48]. Pan C, Zhai J, Wang Z L. Piezotronics and piezo-phototronics of third generation semiconductor nanowires. *Chem Rev* **2019**; 119: 9303-59.

[49]. Zhang Y, Liu Y, Wang Z L. Fundamental theory of piezotronics. *Adv Mater* **2011;** 23: 3004-13.

[50]. Zhang Y, Leng Y, Willatzen M, et al. Theory of piezotronics and piezo-phototronics. *MRS Bull* **2018;** 43: 928-935.

[51]. Yan Z, Hu Y, Shu X, et al. Effects of piezopotential spatial distribution on local contact dictated transport property of ZnO micro/nanowires. *Appl Phys Lett* **2010;** 97: 033509.

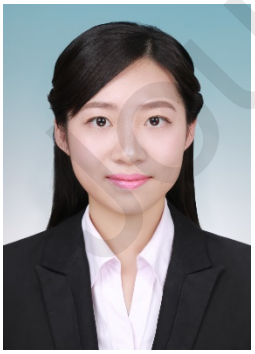

Luming Zhao received her Bachelor's Degree at Huazhong University of Science and Technology in 2014, and Doctor's Degree at Beijing Institute of Nanoenergy and Nanosystems, Chinese Academy of Sciences in 2020. She is currently a Post Doctorate in Beijing Institute of

Basic Medical Sciences. Her research work mainly focuses on triboelectric generator, piezoelectric nanowire device and high sensitive sensors.

Yuxiang Wu received his Bachelor's Degree from Huazhong University of Science and Technology in 2006, and Doctor's Degree from Department of Biomedical Engineering, Huazhong University of Science and Technology in 2011. Currently he is an associate professor in Jianghan University. His research interest includes biomedical monitoring, bioelectronics; wireless sensing; biosensors; nanogenerators, smart wearable device.

Zhou Li received his Bachelor's Degree from Wuhan University in 2004, and Doctor's Degree from Department of Biomedical Engineering, Peking University in 2010. He joined School of Biological Science and Medical Engineering, Beihang University in 2010 as an associate Professor. Currently, he is a professor in Beijing Institute of Nanoenergy and Nanosystems, Chinese Academy of Sciences. His research interest includes nanogenerators, in vivo energy harvesters and self-powered medical devices, biosensors.

摩擦纳米发电机耦合压电效应优化调节肖特基势垒

赵璐明, 李虎, 孟建平, 张岩, 封红青, 吴钰祥, 李舟

肖特基接触传感器已被证明在各种传感系统中具有灵敏度高和响应时间快的优点。为了进一步提高它们的传感性能，需要将半导体和金属电极界面形成的肖特基结的肖特基势垒高度(SBH)调整到合适的范围，以避免 SBH 过高(引起输出过低)或过低(影响器件灵敏度)的情况发生。本文提出了一种简单而有效的通过摩擦纳米发电机(TENG)调节 SBH 的方法，TENG 产生的电压脉冲可有效降低 SBH，SBH 也可在 TENG 停止作用后逐渐恢复。通过将 TENG 处理与压电效应相结合，实现了降低 SBH 的协同效应：与单独的 TENG 处理法和压电效应相比，SBH 的降低量分别增加了 3.8 和 12.8 倍。此外，在压电效应的作用下，经 TENG 处理后降低的 SBH 的恢复时间可以从 1.5 h 缩短到 40 s。该工作证明了一种灵活的 SBH 调节方法, 可以有效地提高肖特基接触传感器和传感系统的灵敏度。本工作也在拓宽肖特基接触电子器件的应用场景方面具有巨大的潜力。

Graphic Abstract

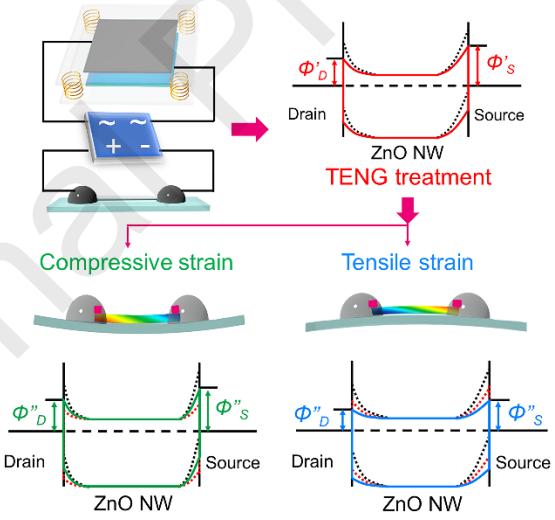

In this work, a flexible and effective SBH tuning method by TENG treatment and its combination with piezotronic effect was demonstrated. A synergistic effect on lowering SBH was achieved, the change of SBH is increased by 3.8 to 12.8 times, compared with dependent TENG treatment and piezotronic effect, respectively. Furthermore, the recovery time of the TENG-lowered SBH can be greatly shortened from 1.5 h to 40 s by piezotronic effect. This

flexible and feasible SBH tuning method can be used to effectively improve the sensitivity of Schottky-contact sensor and sensing system.